

Design of Correcting Mirrors for a Gyrotron Used at Large Helical Device

M.A. Shapiro ¹, T.S. Chu ², D.R. Denison ¹, M. Sato ³, T. Shimozuma ³, and
R.J. Temkin ¹

¹*Plasma Science and Fusion Center
Massachusetts Institute of Technology
Cambridge, MA 02139, USA*

²*Communications and Power Industries
Palo Alto, CA 94303, USA*

³*National Institute for Fusion Science
Gifu-ken 509-52, Japan*

Abstract

We report the design of a mirror correcting system used at the Large Helical Device (LHD) to convert the output radiation of the CPI 84 GHz gyrotron into the HE₁₁ mode of a corrugated waveguide transmission line. The radiation pattern of the gyrotron is measured using an IR camera at LHD. The measured data is analyzed at MIT to retrieve the phase distribution of the radiation. The moments of the measured amplitude arrays are calculated to improve the reliability of the IR images. The retrieved radiation structure is treated to synthesize the correcting mirrors.

1. Introduction

In the LHD experiment, an 84 GHz, 600 kW CPI gyrotron with a single-stage depressed collector [1] is employed for plasma heating. The operating mode of this gyrotron is TE_{15,3}. An improved Vlasov converter of the TE_{15,3} mode into a Gaussian beam is implemented as an output coupler in this tube [2,3]. The waveguide launcher in this mode converter contains two profiled cylindrical mirrors contiguous to the longitudinal edge of the waveguide cut. Such a system of mirrors brings down the losses caused by diffraction in the launcher in the azimuthal plane. The diffraction in the axial plane is presumed to be small because the mode propagation angle is relatively small (36°) in the launcher. A geometric optics approximation is employed to design the mode converter.

An external mirror system including two toroidal mirrors and two flat mirrors was designed and installed at LHD to couple the gyrotron output radiation into a 8.9 cm diameter corrugated waveguide transmission line. It was designed using Gaussian optics assuming that the output radiation is a Gaussian beam. Because of this approximation, 30% power losses occur in the external mirror system.

In this paper we report the gyrotron output radiation measurements and the design of a new external mirror system which efficiently converts this radiation into the HE₁₁ mode of a corrugated waveguide. The designed mirror system including two profiled mirrors, one toroidal and one flat mirror, will replace the existing mirror system. The mirror system design includes the following steps. The gyrotron output radiation is measured at LHD in several positions using an IR camera (Section 2). The IR data are analyzed at MIT to determine those IR images suitable for phase retrieval. The phase distribution is retrieved from the intensity data (Section 3), and the mirror system is synthesized using the MIT codes (Section 4).

These phase retrieval and mirror synthesis codes [4-6] have been employed before to design an external mirror system for a 110 GHz CPI gyrotron installed at General Atomics [5], and also an internal mode converter for a 110 GHz CPI gyrotron with a diamond window [6]. An iterative procedure of phase reconstruction and mirror synthesis [7,8] is utilized in the MIT codes.

2. Infrared Camera Measurements

The IR images from the 84 GHz gyrotron output were taken at LHD using a high resolution (8-bit, 24-dB dynamic range) camera. The schematic of IR measurements is shown in Fig. 2. The paper target was located at the window axis, in 12 positions at distances from the window ranging from 1 to 23 cm. During the IR measurements, the electron beam current of 11 A was maintained, which corresponded to an output power of 150 kW. The pulse width was 3 ms, extended to 4 ms when the target was far from the window. The measurements were made on a single shot basis. The IR camera data include 256×100 arrays of temperature distribution, typically varying from a 21°C minimum to a 93°C maximum, depending on the target position.

Images of a target disk placed at $z=1.10$ cm from the gyrotron window, and four marked reference points placed at $z=10.23$ cm were used to refer to the real coordinates. Using these marked points, the coordinates x and y of the gyrotron window axis on the IR images were determined. This measurement demonstrated that the images were not aligned. Therefore, the IR data coordinates were corrected to have the (0, 0) coordinates at the window axis. However, some of the taken IR images cannot be used for phase retrieval because of the following: (a) inaccuracy of reference point coordinate measurement ; (b) indirect IR rays bouncing in the external mirror box and affecting the IR images.

3. Beam Moments and Phase Retrieval

The measured intensity patterns should be strictly aligned with the accuracy of a fraction of the wavelength in order to avoid errors in the phase retrieval, as demonstrated in [5]. We propose to employ the moments of the IR images to determine whether the IR images are aligned and correspond to a propagation of a real rf beam. Using the measured amplitude distribution $A(x, y)$, we calculate the coordinates $\langle x \rangle$ and $\langle y \rangle$ of the energy center of the image and also the effective radius a_{eff} of the image (dispersion):

$$a_{\text{eff}} = \sqrt{\langle x^2 \rangle + \langle y^2 \rangle - \langle x \rangle^2 - \langle y \rangle^2}, \quad (1)$$

where

$$\langle x^n \rangle = \frac{\int x^n A^2 dx dy}{\int A^2 dx dy}; \quad \langle y^n \rangle = \frac{\int y^n A^2 dx dy}{\int A^2 dx dy}. \quad (2)$$

If an arbitrary shaped quasi-optical rf beam propagates in a uniform medium, according to the theory of moments of quasi-optical beams [9], the beam energy center coordinates vary as a linear function of the axial coordinate z :

$$\langle x(z) \rangle = \langle x(0) \rangle - z \frac{\int A^2 \frac{\partial \Phi}{\partial x} dx dy}{k \int A^2 dx dy}, \quad (3)$$

$$\langle y(z) \rangle = \langle y(0) \rangle - z \frac{\int A^2 \frac{\partial \Phi}{\partial y} dx dy}{k \int A^2 dx dy}, \quad (4)$$

where $\Phi(x, y)$ is the phase distribution and k is the wavenumber. It can be proved the integrals in (3) and (4) do not depend on z , therefore, they can be calculated at $z=0$. The rf beam energy center thus goes straight.

The effective area of the beam evolves as a quadratic function of z [9]:

$$a_{\text{eff}}^2(z) = a_{\text{eff}}^2(0) + B\frac{z}{k} + Cz^2, \quad (5)$$

where B and C are the constants calculated at $z=0$:

$$B = \frac{2 \int A^2(x \frac{\partial \Phi}{\partial x} + y \frac{\partial \Phi}{\partial y}) dx dy}{\int A^2 dx dy} \quad (6)$$

$$C = \frac{\int [(\frac{\partial A}{\partial x})^2 + (\frac{\partial A}{\partial y})^2 + A^2(\frac{\partial \Phi}{\partial x})^2 + A^2(\frac{\partial \Phi}{\partial y})^2] dx dy}{k^2 \int A^2 dx dy}. \quad (7)$$

We calculate coordinates of the energy centers and effective radii of the images (1). Among the IR images taken we choose only those which are aligned. We take the images at 3 planes ($z=8.45$ cm, 16.3 cm, and 19.6 cm from the window) to retrieve the phase. The intensity contour plot is shown in Fig. 3 for the image at Plane 1. Figure 4 plots the energy center coordinates $\langle x \rangle$ and $\langle y \rangle$ and the effective radius a_{eff} for the specified positions of the IR images, and indicates that the images are aligned. We note that the effective area value at $z=19.6$ cm does not fit the quadratic dependence (5). This can be explained by the fact that the pattern is truncated by a $20 \text{ cm} \times 20 \text{ cm}$ paper target dimension used for the IR measurements. Nevertheless, we use this image for the phase retrieval to have at least 3 cm distance between the 2nd and 3rd planes. Otherwise, a 3-plane phase retrieval result would be very close to that obtained with two planes only, which is less determined. The phase distribution retrieved at $z=1$ cm is presented in Fig. 5 by the cuts crossing the phase center at $x=-0.75$ cm and $y=1.6$ cm. The graph in Fig. 5 indicates that the phase front is spherical with some aberrations. We propagate the retrieved field to the check planes at $z=1$ cm, 17.4 cm, and 18.5 cm to compare the calculated and measured amplitude distributions. Good agreement is reached, and the results are plotted in Fig. 6: the measured and retrieved amplitude distributions at $z=18.5$ cm are cut by the lines crossing the energy center ($x=0.06$ cm and $y=1.37$ cm).

4. Correcting Mirror Synthesis

We specify the dimensions of the mirrors $20 \times 20 \text{ cm}^2$; Mirror 1 is placed at $z=27.6$ cm from the window, and Mirrors 1 and 2 are spaced by 24 cm. To get better performance, we filter the amplitude distribution at Mirror 1, such that the maximum spatial harmonic propagation angle is 40° . This angle is consistent with the maximum propagation angle of the ray bouncing between Mirrors 1 and 2. The amplitude distribution on Mirror 1 is plotted in Fig. 7.

We take the calculated pattern at Mirror 1 and a Gaussian pattern at Mirror 2, and run the synthesis code to calculate the profile of Mirror 1 [6]. Since the mirror synthesis procedure is based on a phase corrector approximation, we check the synthesis result using an independent MIT physical optics code [10] to propagate the retrieved beam to Mirror 1, reflect the beam from Mirror 1 and propagate it farther to the Mirror 2 position. We compare the pattern at Mirror 2 to that used for the synthesis of Mirror 1.

It turns out that the best performance in the mirror synthesis is obtained if the Gaussian amplitude imposed on Mirror 2 matches the Mirror 1 amplitude distribution. So,

at Mirror 2, we specify the Gaussian distribution with the center coordinates ($\langle x \rangle = 0.2$ cm and $\langle y \rangle = 1.4$ cm) and effective x and y dimensions of $W_x = 2\sqrt{\langle x^2 \rangle - \langle x \rangle^2} = 5.9$ cm and $W_y = 2\sqrt{\langle y^2 \rangle - \langle y \rangle^2} = 7.6$ cm the same as at Mirror 1. Figure 8 shows the contour plot of the amplitude imposed at Mirror 2 (dashed lines) as well as the pattern at Mirror 2 calculated using the physical optics code and filtered (solid lines). Thus, Mirror 1 is synthesized, and then the amplitude and phase distributions simulated using the physical optics code at the Mirror 2 position are employed to synthesize the Mirror 2 profile.

The Gaussian beam optimal for excitation of the HE_{11} mode has a flat phase front at the waveguide aperture and the waist dimension of $W = 2.84$ cm. Using Gaussian optics we propagate this Gaussian beam to the position of the Mirror 3 (at 41.3 cm from the waveguide aperture).

To synthesize Mirror 2, we impose this Gaussian amplitude at Mirror 3 and the amplitude at Mirror 2 simulated by the physical optics code. Taking the distance of 50 cm between Mirror 2 and Mirror 3, we synthesize Mirror 2. Mirrors 1 and 2 are concave, and their profiles are plotted in Figs. 9 and 10 respectively.

Mirror 3 is toroidal and aimed to match the output from the two mirror system to the corrugated waveguide mode, and Mirror 4 is flat and just changes the direction of propagation. The shape of the toroidal Mirror 3 is determined using Gaussian optics and optimized using physical optics code runs to get the HE_{11} mode field distribution at the waveguide. Mirror 3 is convex, and its curvature radii are 306 cm in the plane of Fig. 1, and 83 cm in the perpendicular plane.

The result of propagation of the retrieved beam through the designed system of mirrors to the waveguide aperture is shown in Fig. 11. The analysis of the amplitude and phase distributions at the waveguide aperture indicates that it is a 94% Gaussian beam with the waist matching the HE_{11} mode, and with a slightly curved phase front: the minimum phase front curvature radius is 230 cm.

To appreciate the mirror system performance we note that the retrieved output radiation of the gyrotron is a poor Gaussian beam; only 74% of the power is in a Gaussian component.

Conclusions

We designed a new mirror system to convert the output radiation of the 84 GHz gyrotron at LHD into the corrugated waveguide mode. The mirror system includes 4 mirrors: 2 profiled, 1 toroidal and 1 flat. The design is based on the IR measurements made at LHD using a high-resolution IR camera. The problem of misalignment of IR images arises when the raw data are employed to retrieve the phase from the intensity measurements. The images have to be corrected or validated to be useful for phase retrieval. We demonstrate that this correction can be done by calculating the moments of IR images. We use a new approach for mirror synthesis which includes the matching of patterns at Mirrors 1 and 2. We calculate a high efficiency (94%) of conversion into the Gaussian beam matching the corrugated waveguide mode.

The work of the US participants is supported by the Department of Energy.

References

- [1] T. Shimozuma, M. Sato, Y. Takita, S. Ito, S. Kubo, H. Idei, K. Ohkubo, T. Watari, T.S. Chu, K. Felch, P. Cahalan, C.M. Loring, Conf. Digest, 22nd Int. Conf. on Infrared and Millimeter Waves, Wintergreen (1997) p. 194.

- [2] M. Sato, T. Shimosuma, S. Kubo, Y. Takita, Y. Tsubokawa, K. Ohkubo, T. Kuroda, H. Huey, H. Jory, *Fusion Eng. Design* 26 (1995) 287.
- [3] M. Iima, M. Sato, Y. Amano, S. Kobayashi, M. Nakajima, M. Hashimoto, O. Wada, K. Sakamoto, M. Shiho, T. Nagashima, M. Thumm, A. Jacobs, W. Kasperek, *Conf. Digest, 14th Int. Conf. on Infrared and Millimeter Waves, Wurzburg* (1989) p. 405.
- [4] D.R. Denison, T. Kimura, M.A. Shapiro, R.J. Temkin, *Conf. Digest, 22nd Int. Conf. on Infrared and Millimeter Waves, Wintergreen* (1997) p. 81.
- [5] D.R. Denison, PhD Thesis, MIT (1999).
- [6] D.R. Denison, T.S. Chu, M.A. Shapiro, R.J. Temkin, *IEEE Trans. Plasma Sci.* 27 (1999) 512.
- [7] A.V. Chirkov, G.G. Denisov, N.L. Aleksandrov, *Optics Commun.* 115 (1995) 449.
- [8] A.A. Bogdashov, A.V. Chirkov, G.G. Denisov, D.V. Vinogradov, A.N. Kuftin, V.I. Malygin, V.E. Zapevalov, *Int. Journ. Infrared and Millimeter Waves* 16 (1995) 735.
- [9] S.N. Vlasov, V.A. Petrishchev, V.I. Talanov, *Izvestiya Vysshikh Uchebnykh Zavedenii Radiofizika* 14 (9) (1971) 1353.
- [10] M. Blank, K. Kreischer, R.J. Temkin, *IEEE Trans. Plasma Sci.* 24 (1996) 1058.

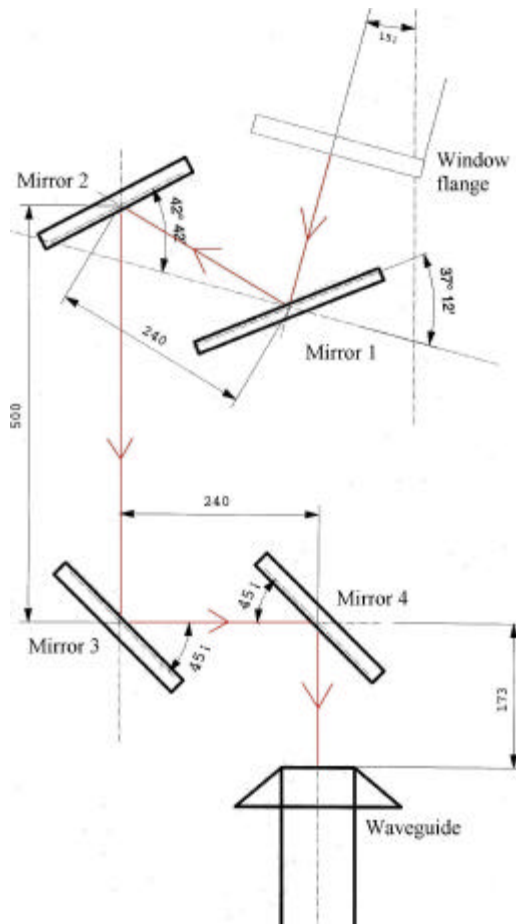


Fig.1. Mirror system schematic.

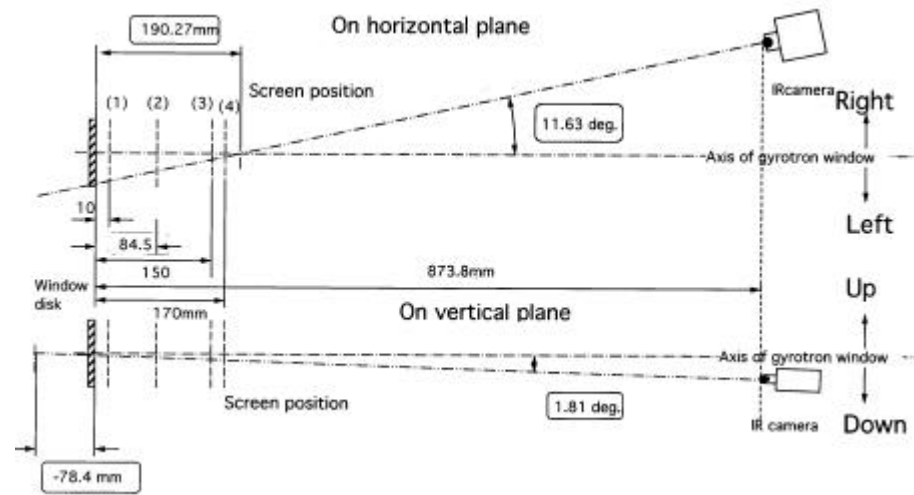


Fig.2. Schematic of infrared camera measurements.

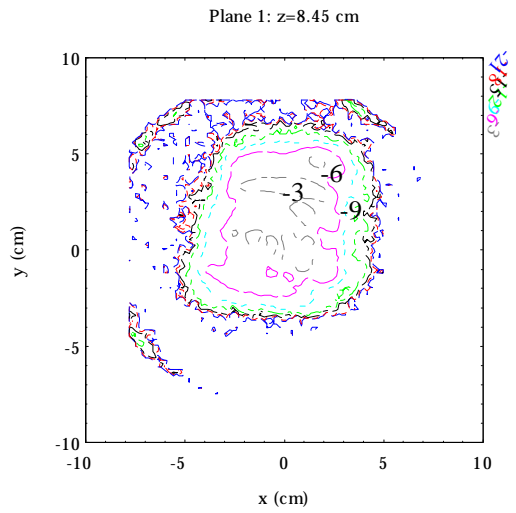


Fig. 3. Example of an infrared image used for phase retrieval: amplitude contours from -3 dB up to -21 dB with a 3-dB interval.

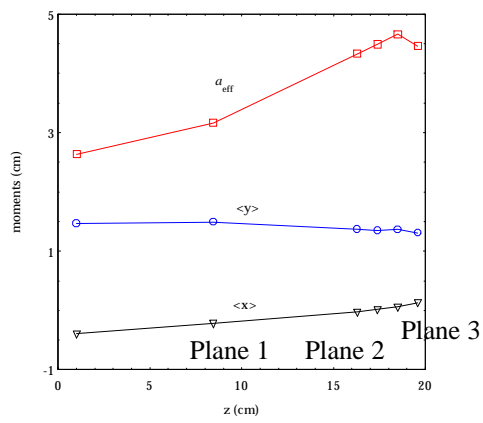


Fig. 4. Moments of the IR images used for phase retrieval (Planes 1, 2, and 3) and for checking the phase retrieval result.

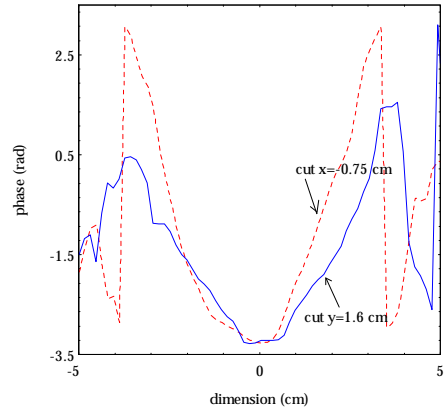


Fig. 5. Phase distribution retrieved at $z=1$ cm from the window: cuts along the phase center coordinates $x=-0.75$ cm and $y=1.6$ cm .

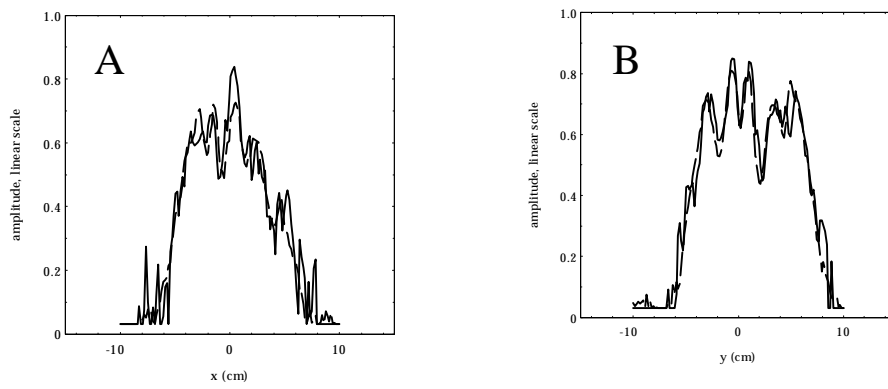


Fig. 6. Measured (solid line) and retrieved (dashed line) amplitude distributions at the check plane $z=18.5$ cm: $y=1.37$ cm – cut (A) and $x=0.06$ cm – cut (B).

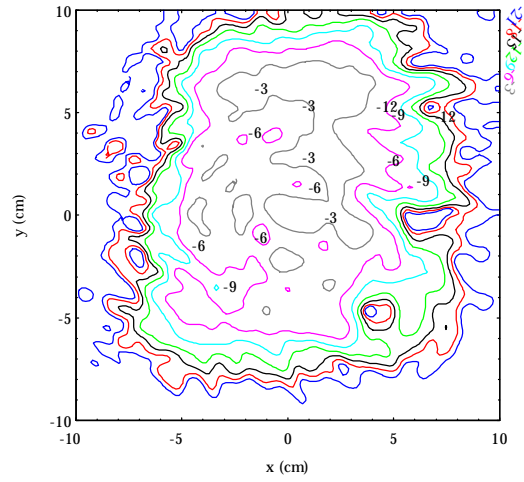


Fig. 7. Pattern calculated at the Mirror 1 position, at $z=27.6$ cm from the gyrotron window: contour plot in dB .

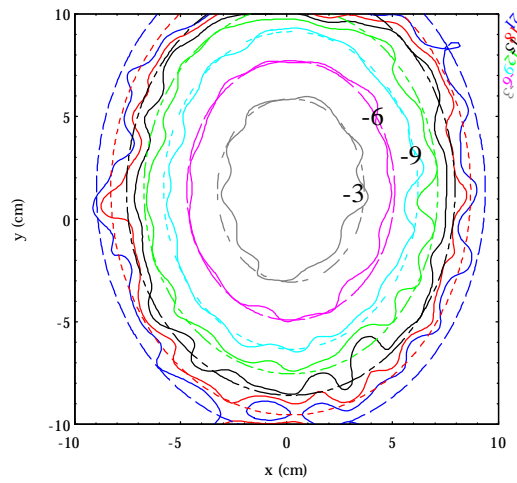


Fig. 8. Pattern at Mirror 2: dashed – used in mirror synthesis, solid – obtained using the physical optics code.

Fig. 9. Mirror 1 profile

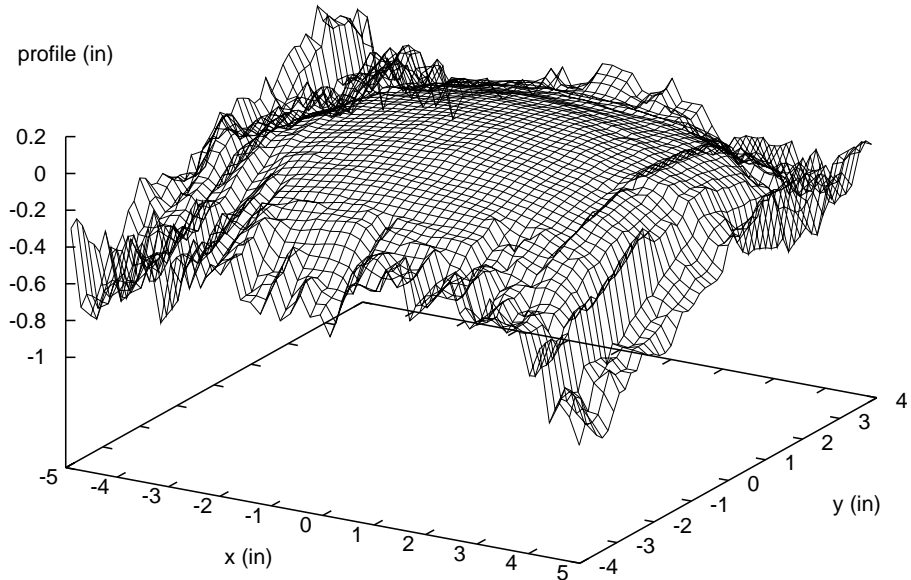
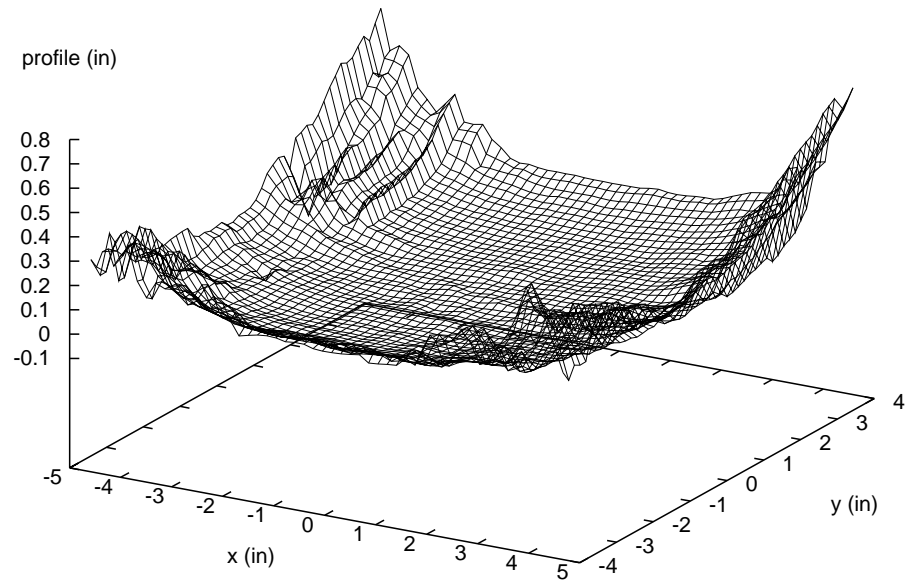


Fig. 10. Mirror 2 profile



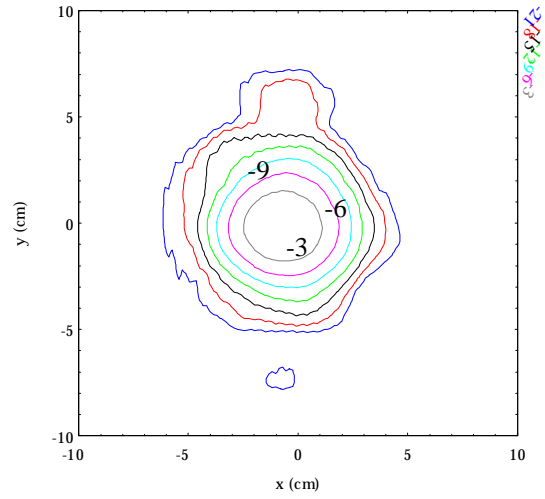


Fig. 11. Physical optics propagation code result: pattern at the waveguide aperture, contours from -3 dB up to -21 dB.